R-JET: A postprocessing code for radiative transport in relativistic jets

Kouichi HIROTANI (ASIAA)

H. Shang, R. Krasnopolsky (ASIAA),

K. Nishikawa (Alabama Univ)

September 15, 2025

Jeju Island, South Korea

§1 Energy extraction from rotating black holes

Every active galaxy harbors a SMBH ($10^6\ M_\odot$-$10^{9.5} M_\odot$).

E.g., Ferrarese+'96, ApJ 470, 444; Larkin+'16,MN 462,1864

EHT (Event Horizon Telescope) project (2020-)

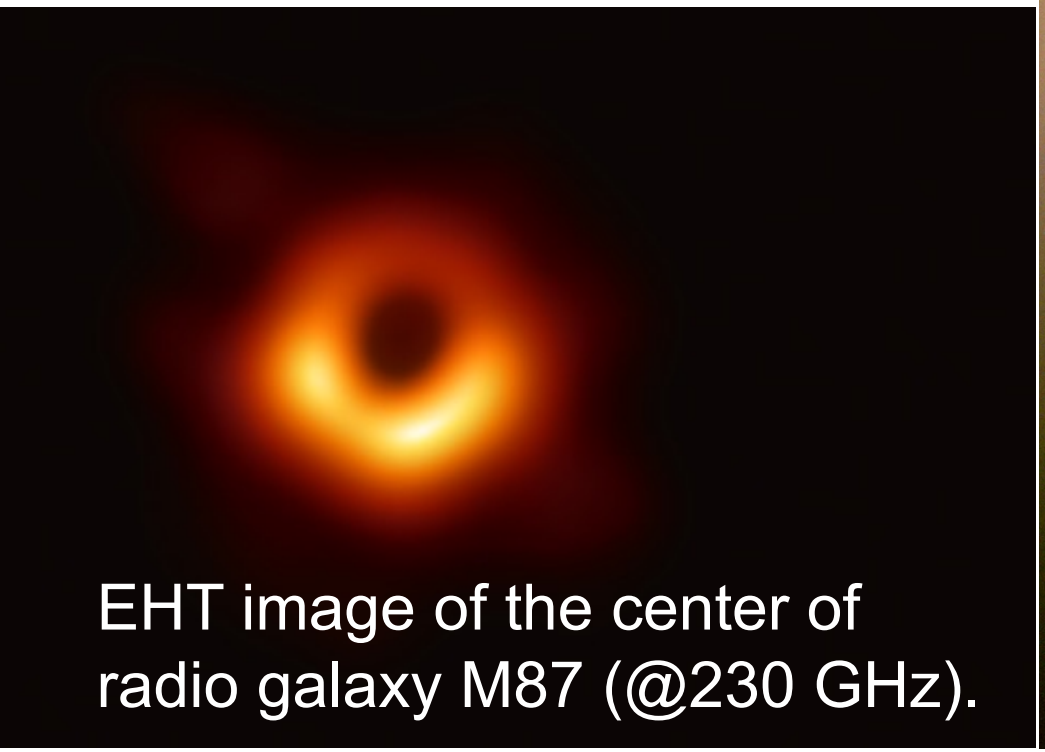

EHT image of the center of radio galaxy M87 (@230 GHz).

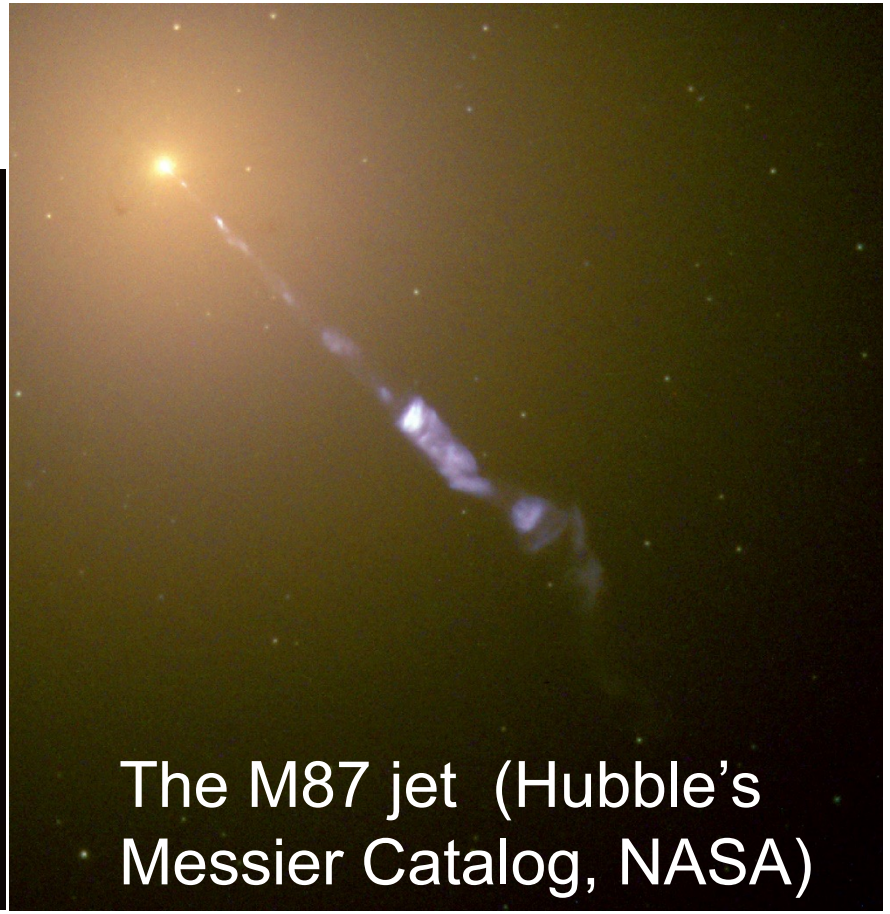

The M87 jet (Hubble's Messier Catalog, NASA)

M87: ideal laboratory

Messier 87 (M87) is an ideal laboratory for the study of extra-galactic jets from low-accreting AGNs.

- Small distance (*d=16.7* Mpc; Blakeslee + 2009)
- Large BH mass ($\sim 6.6\times10^{9}M_{\odot}$; Gebhardt + 2011; EHT Collaboration + 2019a).

In radio frequencies, high-resolution VLBI imaging of the inner jet regions provides the best constraints for the jet formation theories.

M87: ideal laboratory

It has been revealed that the M87 jet has a wide opening angle of $\sim 60^\circ$ on sub-pc scales (Junor et al. 1999) before expanding quasi-parabolically out to $d \sim 10^5 R_S$ from the core (Asada & Nakamura 2012).

R_S : Schwarzschild radius

Moreover, a limb-brightened structure is found on pc and sub-pc scales at 15 GHz (Kovalev + 2007), 43 GHz (Ly + 2007), and 86 GHz (Hada + 2016; Lu + 2023).

At 230 GHz, EHT revealed the center of the M87 galaxy and reported a ring-like structure with a diameter ($\sim 5\ R_S$) (EHT Collaboration 2019b).

M87: ideal laboratory

The ring-like structure was also confirmed at 86 GHz with a greater diameter $\approx 8.4R_S$. (Lu + 2023). In their work, the limb-brightened structure extends down to the projected distance of 0.1 mas from the core (i.e., a de-projected distance ~ $45R_S$ from the ring center).

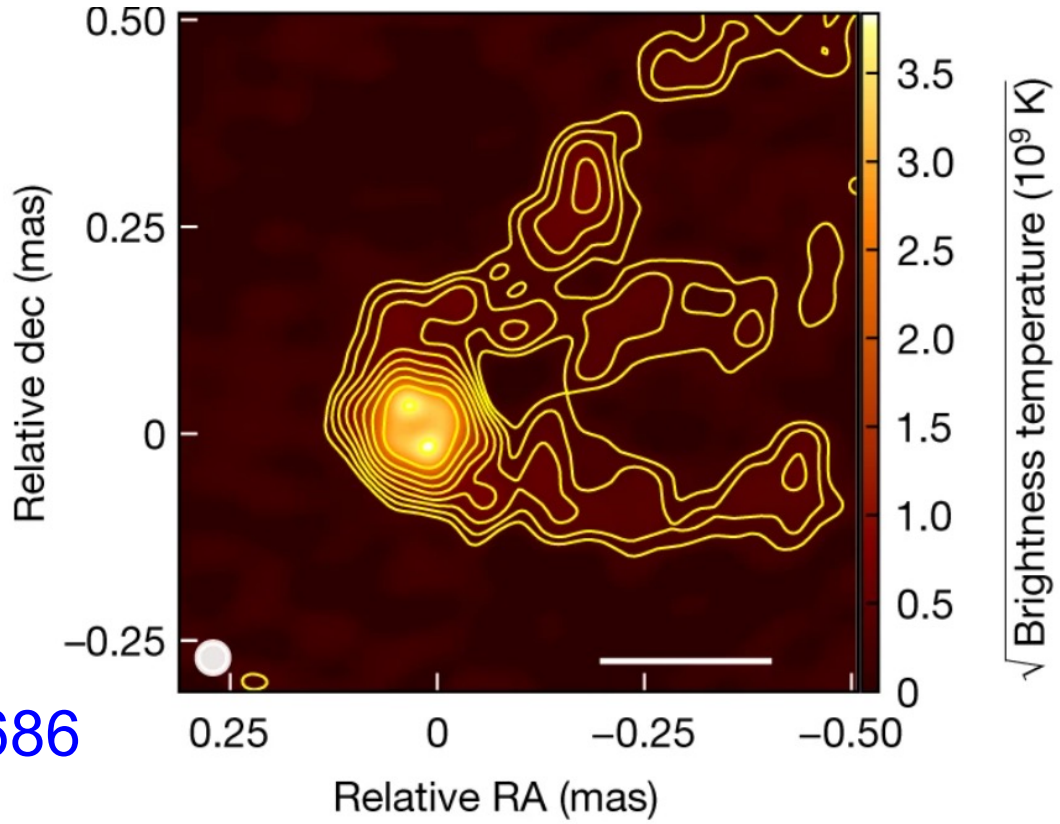

Fig.) Triple-peaked profile of the M87 jet @ $r < 100\ R_S$

Lu+ 2023, Nature 616, 686

Theoretical models for the M87 jet

Fuentes et al. (2018) investigated jet transverse structures of over-pressured super-fast-manetosonic jet.

Takahashi et al. (2018) reproduced limb-brightened struct., assuming a ring-like distribution of emitting electrons.

Ogihara et al. (2019) examined a force-free model to find that the density near the edge produces the bright limbs.

Kramer & MacDonald (2021) solved polarized radiative transfer to find that the jet becomes limb-brightened when the magnetic field is toroidally dominated, and spine-brightened when the field is poloidally dominated.

Frolova et al. (2023) examined MHD models to show that triple-peaked profile constrains the fraction of leptons.

Energy extraction from rotating BHs

In recent two decades, GRMHD simulations demonstrated that these relativistic flows can be fueled by an extraction of the BH's rotational energy, i.e., by the "Blandford-Znajek (BZ) process"

(Blandford & Znajek 1977; Koide + 2002; McKinney + 2005; Tchekhovskoy + 2010, 2011).

The BZ process is driven when the horizon-crossing magnetic field is dragged in the direction of the BH's spin.

The resulting Lorentz force $(c/4\pi)(\nabla \times B)^{\theta} \times B^{r}$ generates a counter torque on the event horizon.

The extracted BH's rotational energy is carried away as torsional Alfven waves (i.e., as a Poynting flux).

R-JET: a post-processing radiative transport code

The extracted EM energy can be transformed into kinetic and internal energies of $e^{\pm}$'s at some distance from the BH, and eventually emitted as radiation.

We thus semi-analytically examine the jet emission by connecting the jet-launching and jet-downstream regions, using our post-processing, un-polarized radiative transfer code **R-JET** (KH + 2025a, ApJ 984, 16).

Today, we apply the **R-JET** code to the **M87** jet, focusing on the spectral energy distribution (SED) and coreshift of the synchrotron emission. It is demonstrated that these two observables strongly constrain the jet parameters. (KH + 2025b, ApJ in press).

§2 The R-JET code: Parabolic Jet Model

To model stationary and axisymmetric jets, we model the flow lines with a parabolic-like geometry

(Broderic & Loeb 2009; Takahashi + 2018)

$$\text{Magnetic flux function: } A_\varphi = A_{\max}\left(\frac{r}{r_{\rm H}}\right)^q\left(1-\left|\cos\theta\right|\right)$$

where $r_{\rm H} = M + \sqrt{M^2 - a^2}$ denotes the horizon radius.

For the M87 jet, a quasi-parabolic flow line, $q=0.75$, is reported within de-projected altitude $10^{1.2} < r/R_{\rm S} < 10^{5.3}$ (Asada & Nakamura 2012; Asada + 2016).

Jet boundary is defined by $A_\varphi = A_{\max}$.

§2 The R-JET code: Parabolic Jet Model

The EM energy and momentum is carried along each magnetic flux tube (A_φ = const.) as the Poynting flux,

$$T^r{}_t = \frac{1}{4\pi}\left[F^{r\alpha}F_{\alpha t} + \frac{1}{4} g_t^{\ \mu} F^{\alpha\beta}F_{\partial\alpha\beta} \right] = \frac{1}{4\pi} \underline{F^{r\theta}F_{\theta t}} \quad (\mathrm{E}_\theta \times \mathrm{B}_\varphi)$$

where $F_{\mu\nu}$ denotes the Faraday tensor. The BH's rotational energy is extracted via the Blandford-Znajek mechanism (Tchekhovskoy et al. 2010)

$$T^r{}_t{}^{(0)} \approx \frac{3}{4\pi^2} \sin\left[\frac{\pi}{2}(1-\cos\theta)\right] \Omega_F \left(\omega_H - \Omega_F\right) {B_{p,H}}^2$$

θ dependence

where $B_{p,H}$=B_{p}(r=r_{H}).

§2 The R-JET code: Parabolic Jet Model

The BH's rotational energy can be electromagnetically extracted. In this case, the Poynting flux preferentially concentrates along the magnetic-field lines threading the horizon in the lower latitudes (i.e., near the equator).

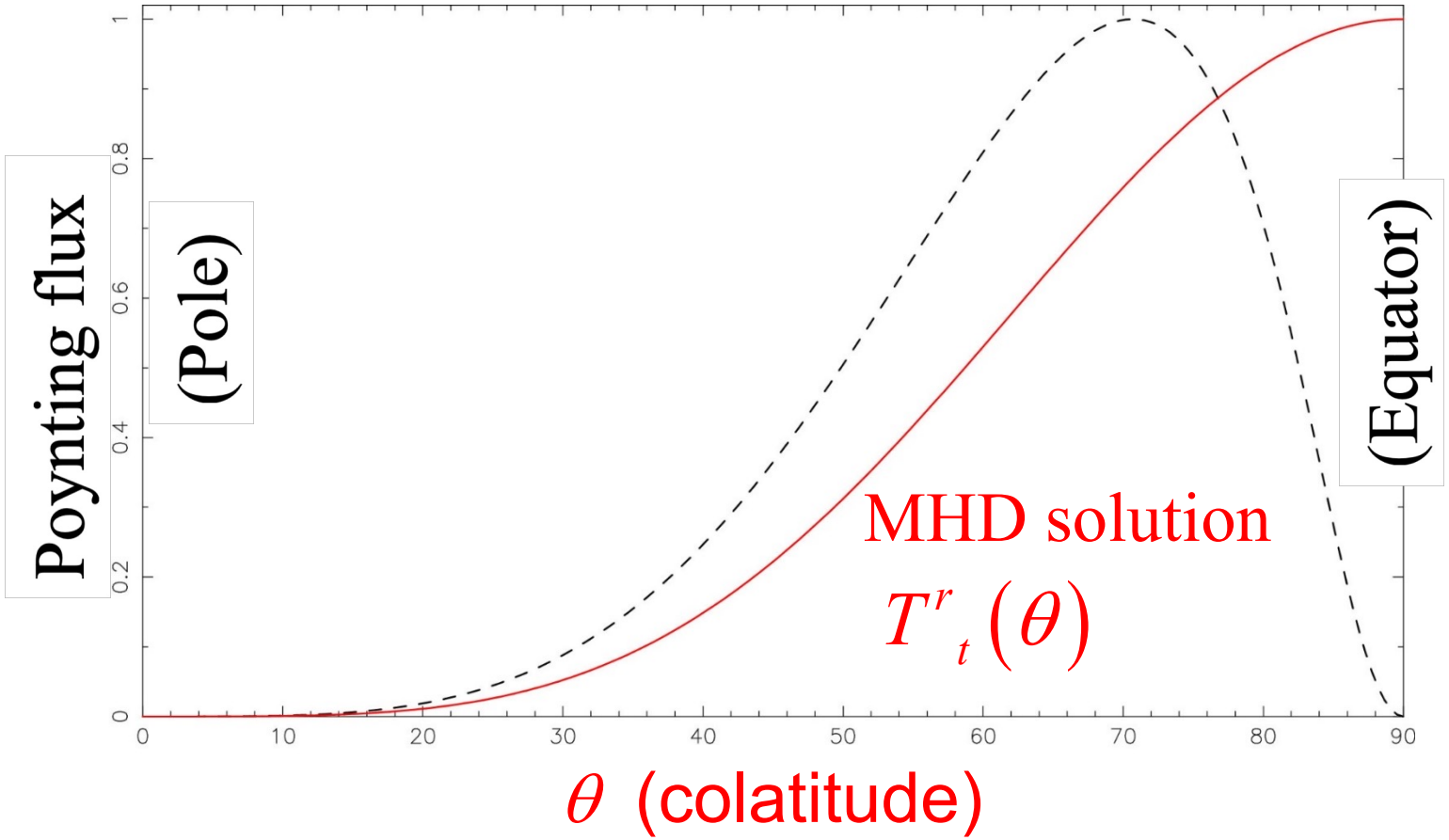

§2 R-JET code: Emission & absorption coefficients

It is possible that these EM energies are turned into kinetic or internal energies at large distances.

In AGN jets, *Kinetic energies » radiated energies* (Celloti & Fabian 1993, MNRAS 264, 228).

In the **R-JET** code, we thus constrain the kinetic energy flux by imposing the conservation of (Poynting + kinetic) energy along each magnetic flux tube. Using the magnetization parameter σ (ratio of EM & kinetic fluxes), we can express the kinetic energy flux as

$$F_{\rm kin} = \frac{1}{1+\sigma}\frac{B_p(r,\theta)}{B_p^{(0)}} T^{r}_{t}{}^{(0)}$$

§ 2 R-JET: Electron density at each point

Introducing the nonthermal fraction ζ of leptons, we an alternatively express the kinetic flux as

$$F_{\rm kin} = c\Gamma(\Gamma-1)\left[\zeta\langle\gamma_-\rangle+\frac{3}{2}(1-\zeta)\Theta\right]n_* m_e c^2$$

Total energy density in coming frame

Γ : bulk Lorentz factor

$\langle\gamma_-\rangle$: mean Lorentz factor of nonthermal leptons

§ 2 R-JET: Electron density at each point

$$F_{\rm kin} = c\Gamma(\Gamma-1)\left[\zeta\left\langle\gamma_{-}\right\rangle+(1-\zeta)\Theta\right]n_{*}m_{e}c^{2}$$

$$F_{\rm kin} = \frac{1}{1+\sigma}\frac{B_{p}(r,\theta)}{B_{p}^{(0)}}F_{\rm BZ}^{(0)}$$

R-JET code:

Thus, if we impose the Poynting flux $F_{\rm BZ}^{(0)}$ at the jet launching point, $r=R_{\rm S}$, and constrain the evolution of σ and Γ, we obtain the electron density n_{*}.

Then we can compute the emission and absorption coefficients at each position in the jet, and depict the VLBI map of a jet.

§ 2 R-JET: Emission & absorption coefficients

Non-thermal $e^{\pm}$'s

Power-law energy distribution (*: measured in jet frame)

$$\frac{dn_*}{d\gamma} = n_0 \gamma^{-p} \rightarrow n_* = \int_{\gamma_{\min}}^{\gamma_{\max}} \frac{dn_*}{d\gamma} d\gamma = \frac{\gamma_{\max}^{1-p} - \gamma_{\min}^{1-p}}{p-1} n_0$$

Emission coefficient

$$j_\nu^* = \frac{\sqrt{3}}{2} \frac{e^2}{c} \nu_L n_0 \frac{\Gamma\left(\frac{p}{4} + \frac{19}{12}\right)\Gamma\left(\frac{p}{4} - \frac{1}{12}\right)}{p+1} \left(\frac{1}{3}\frac{\nu_*}{\nu_L}\right)^{-\frac{p-1}{2}}$$

$$\nu_L \equiv \frac{eB_* \sin\chi}{2\pi m_e c} = 2.799 \times 10^6 B_* \sin\chi \text{ Hz}$$

§ 2 R-JET: Emission & absorption coefficients

Non-thermal $e^{\pm}$'s

Absorption coefficient

$$\alpha_\nu^{*} = C(p) r_0^{\,2} n_0 \frac{\nu_0}{\nu_*} \left(\frac{\nu_B}{\nu_*} \right)^{1+\frac{p}{2}}$$

p	2.0	3.0	4.0
$C(p)$	1.39	2.09	3.67

Optically thin spectral index, $\alpha = \dfrac{1-p}{2}$

Gyro freq.

$$\nu_B \equiv \frac{eB_*}{2\pi m_e c} = \frac{\nu_L}{\sin\chi}$$

(good estimate: $\chi \sim 60^{\circ}$)

$$\nu = \frac{\delta}{1+z}\nu_*$$

$$\delta \equiv \frac{1}{\Gamma(1-\beta\cos\varphi)}$$

ν : observer's frequency

ν_* : co-moving frequency

φ : viewing angle

§ 2 R-JET: Emission & absorption coefficients

Thermal $e^{\pm}$'s (We assume Maxwell-Jüttner distribution)

Emission coefficient (Wardzinski + 2011, MNRAS 314, 183)

$$j_\nu^{*} \approx \frac{2\sqrt{2}\pi}{27}\frac{\Theta^2}{K_2(\Theta^{-1})}\frac{e^2}{c}\nu_L n_* X^{\frac{1}{3}}\left(X^{\frac{1}{3}}+2^{\frac{11}{12}}\right)^2 \exp\left(-X^{\frac{1}{3}}\right)$$

$$\Theta \equiv \frac{kT}{m_e c}, \quad X \equiv \frac{\nu_*}{\nu_S}, \quad \nu_S \equiv \frac{2}{9}\nu_L \Theta^2 \sin\chi$$

Absorption coefficient (Kirchhof's law)

$$\alpha_\nu^{*} = \frac{j_\nu^{*}}{B_\nu(T)}, \quad B_\nu(T) \approx I_{\nu^*}^{RJ}(T) = \frac{2\nu_*^{\,2}}{c^2}kT = 2m_e\nu_*^{\,2}\Theta$$

§ 2 R-JET: Emission & absorption coefficients

Solve the unpolarized radiative transfer equation

$$\frac{dI_\nu}{ds} = j_\nu - \alpha_\nu I_\nu$$

in the observer's frame
(from the source to the observer).

§2 R-JET: Lorentz factor & magnetization parameter

Apply the **R-JET** code to the M87 jet.

To constrain $\Gamma(r)$ and $\sigma(r)$, we employ MHD simulation by Mertens et al. (2016, AA 595, 54).

Combining $\Gamma(r)$ and $\sigma(r)$, with the above-mentioned Poynting flux (normalization & θ dependence), we can constrain the electron density at each position in the jet.

Normalization of the Poynting flux can be translated into the magnetic field strength at the event horizon.

Thus, adjusting the magnetic-field strength and the nonthermal fraction of electrons, we can compute the SED and the core shift, and compare them with observations.

§3 Results: SED of M87 jet

The best-fit SED is obtained when $B_p = 25$ G @ $r = R_S$, $q = 0.75$ (consistent with VLBI obs. at greater scales).

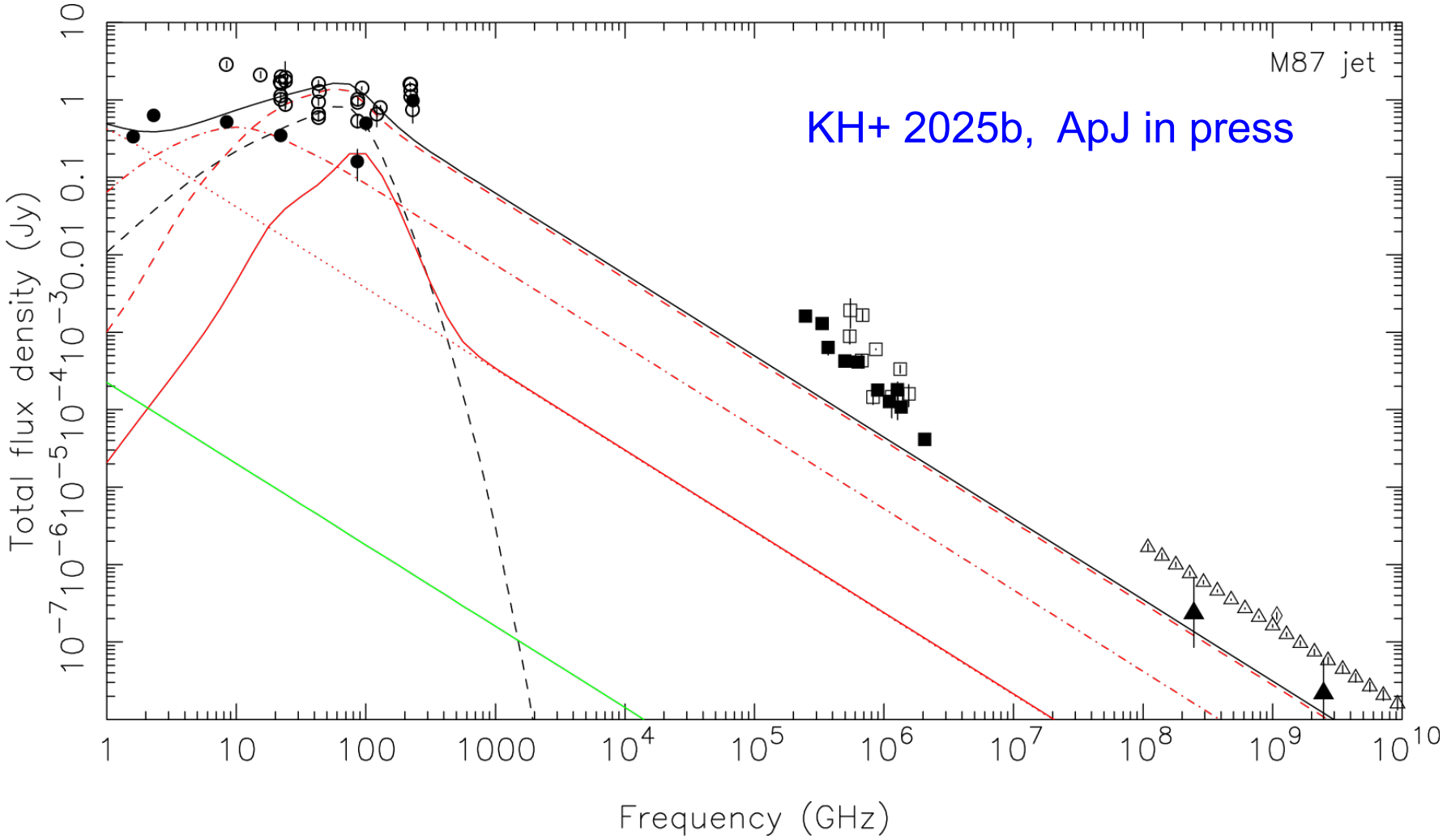

§3 Results: SED of M87 jet

The best-fit SED is obtained when $B_p = 25$ G @ $r = R_S$, $q = 0.75$ (consistent with VLBI obs. at greater scales).

The nonthermal fraction of $e^{\pm}$'s is adjusted so that both SED and core shift may match observations.

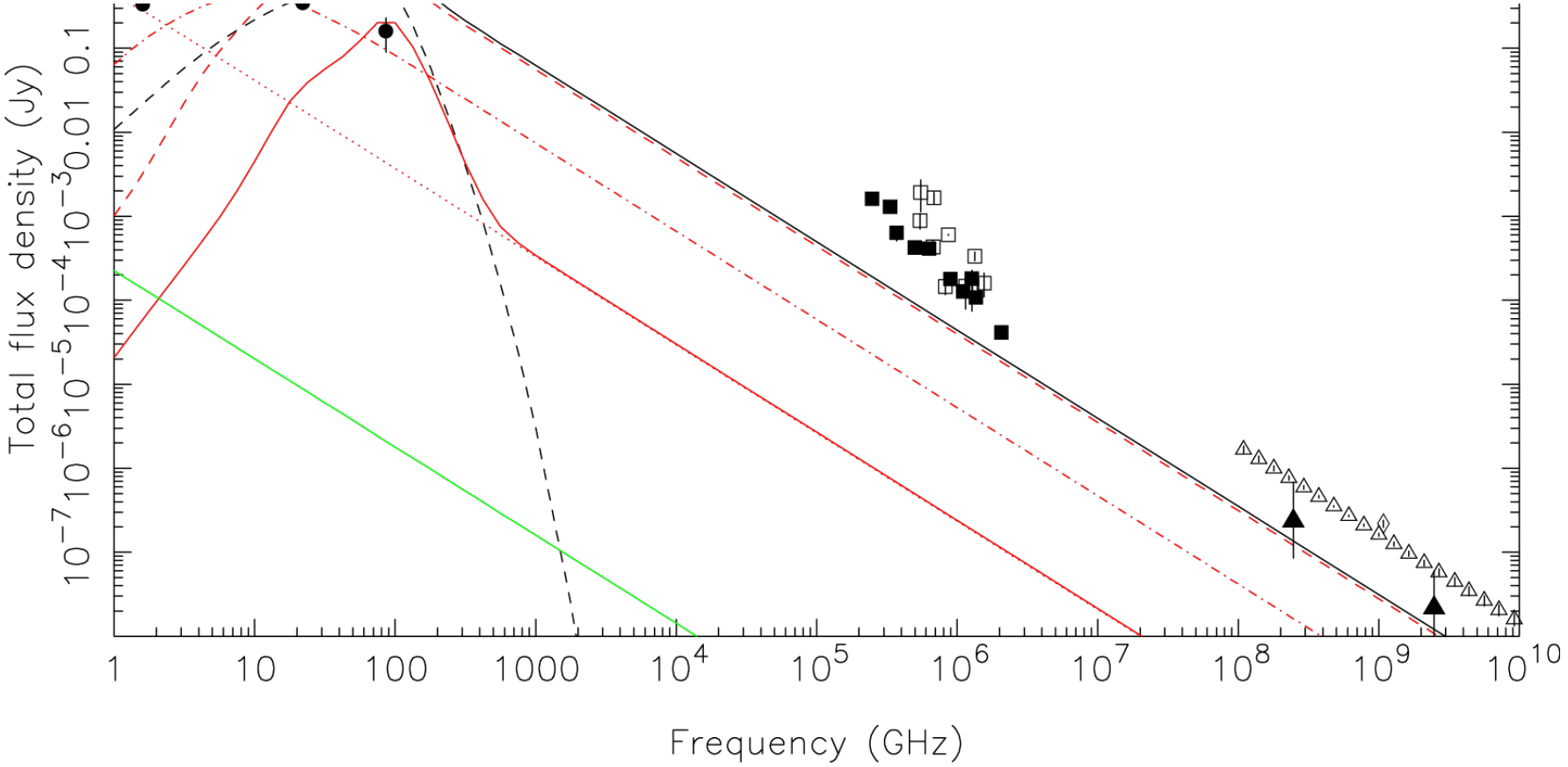

§3 Results: Core shift of M87 jet

The same parameter set gives a consistent core shift (due to opacity effect) with VLBI observations.

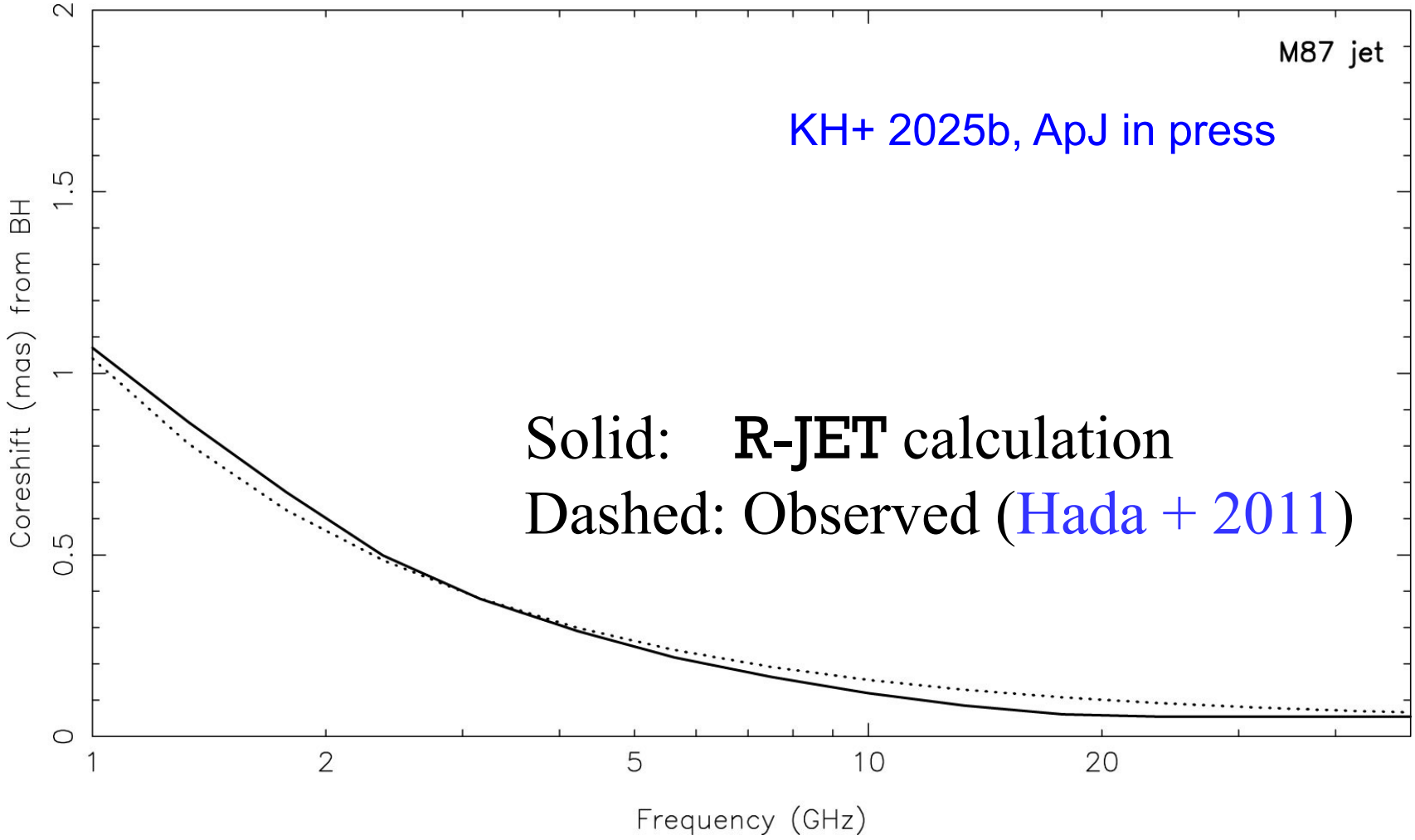

§3 Results: formation of ring-like structure

The jet-launching altitude ($r=6.8R_S$) is adjusted so that the predicted ring-like structure may have the same diameter (64 μas) as reported by Lu + (2023).

Middle/low-latitude concentration of the BZ flux results in this ring-like structure.

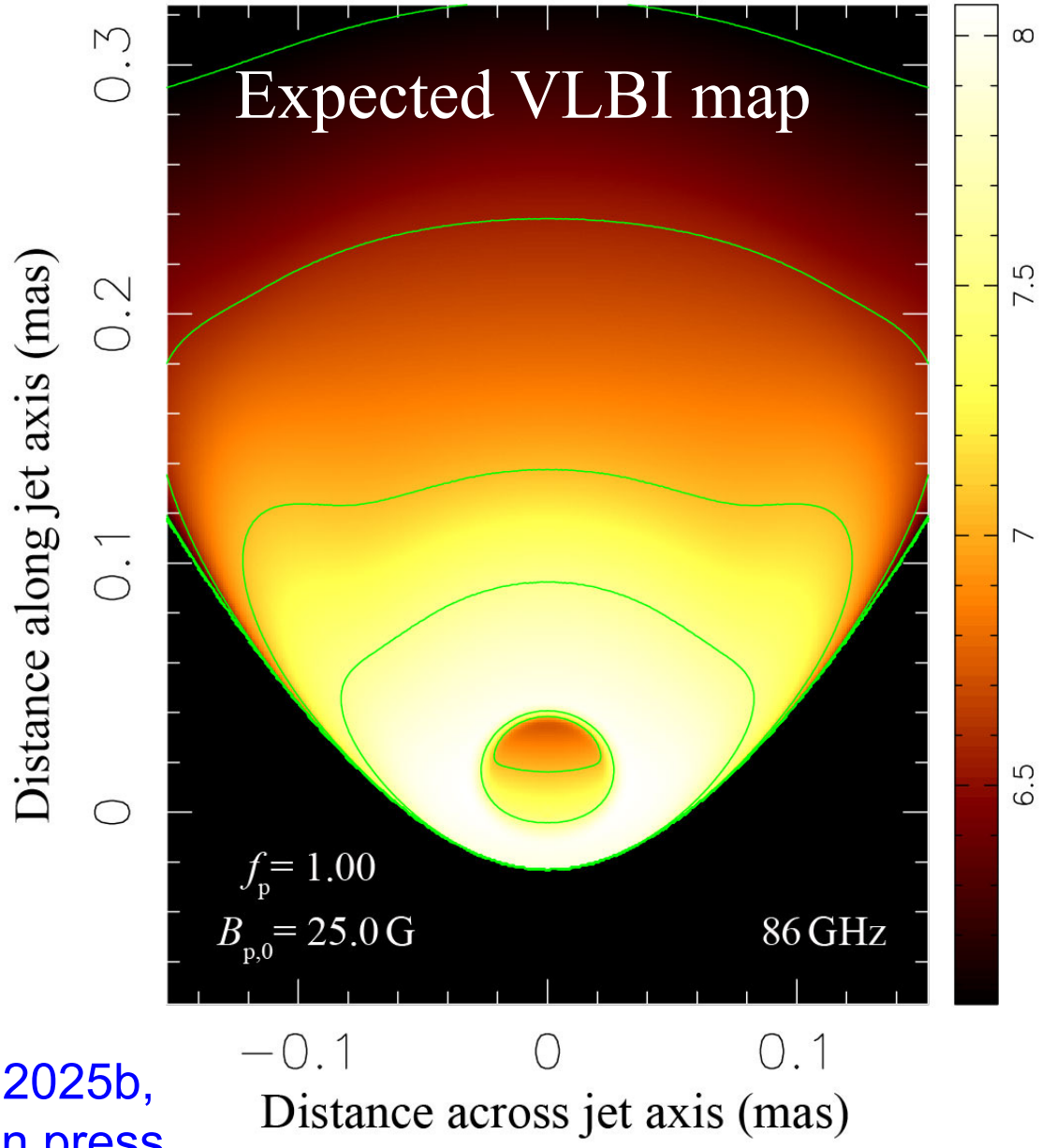

KH+ 2025b, ApJ in press

§3 Results: formation of limb-brightened jets

Let us change the impact of composition.

Fig: general case ($M = 10^9 M_\odot$). f_p: pair fraction

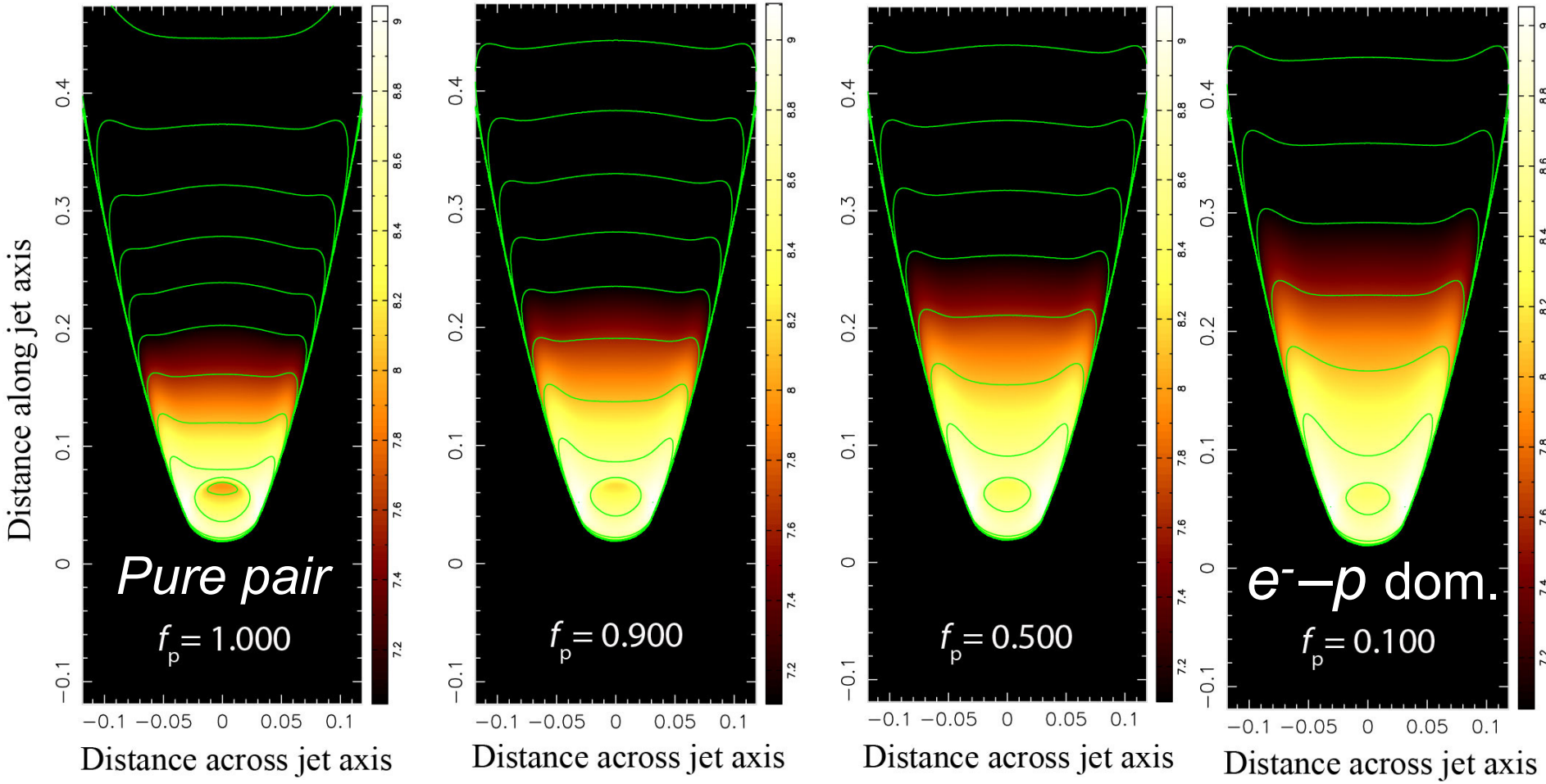

§3 Results: formation of limb-brightened jets

Ring-like structure is enhanced when the plasma composition is pair-dominated.

Limb-brightened structure is enhanced when it is normal-plasma-dominated.

KH+ 2025a, ApJ 984, 16

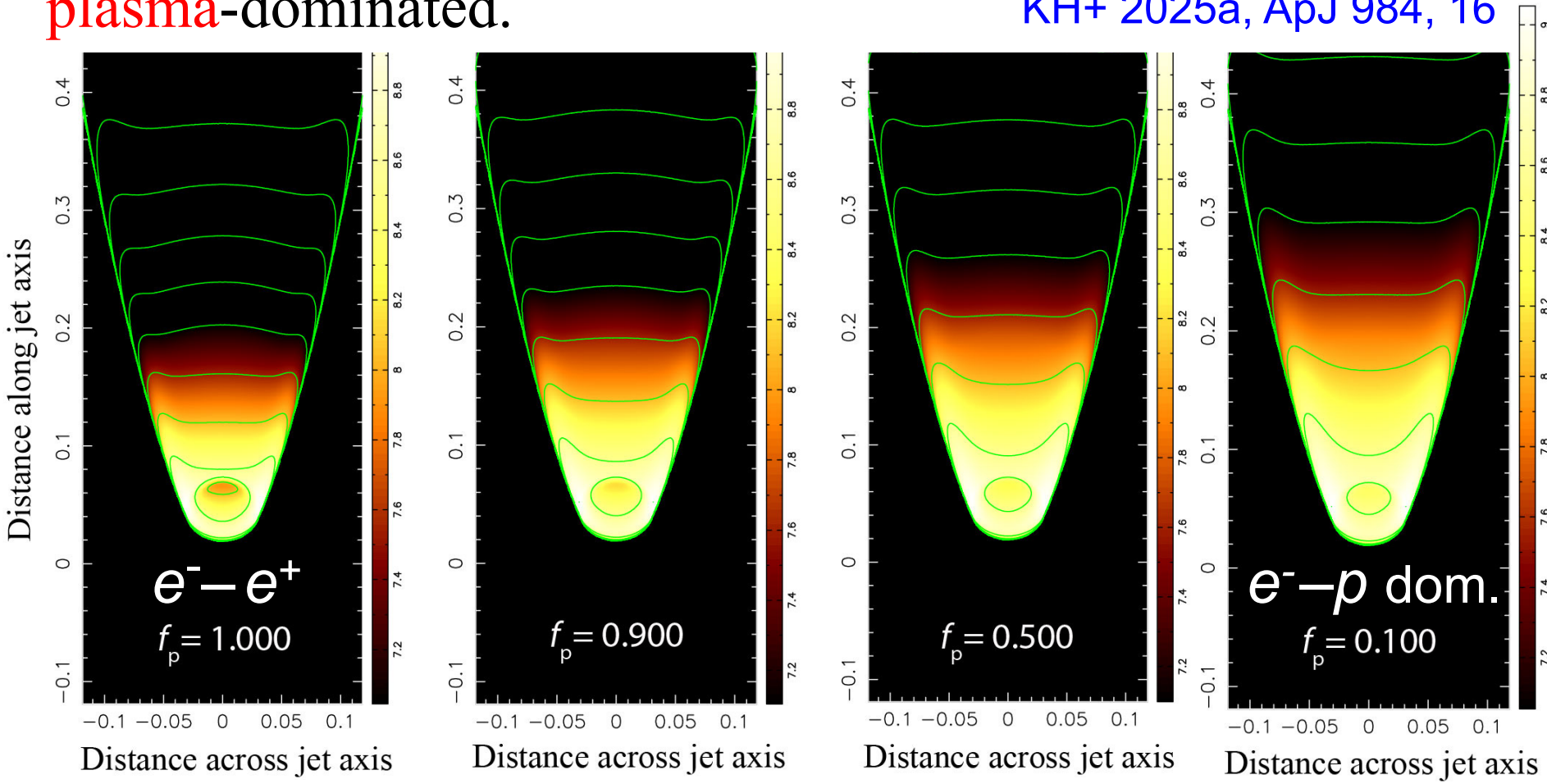

§3 Results: SED vs. plasma composition

SED peaks in sub-mm wave lengths by the thermal emission near the jet base. The peak becomes prominent as the jet becomes normal-plasma-dominated.

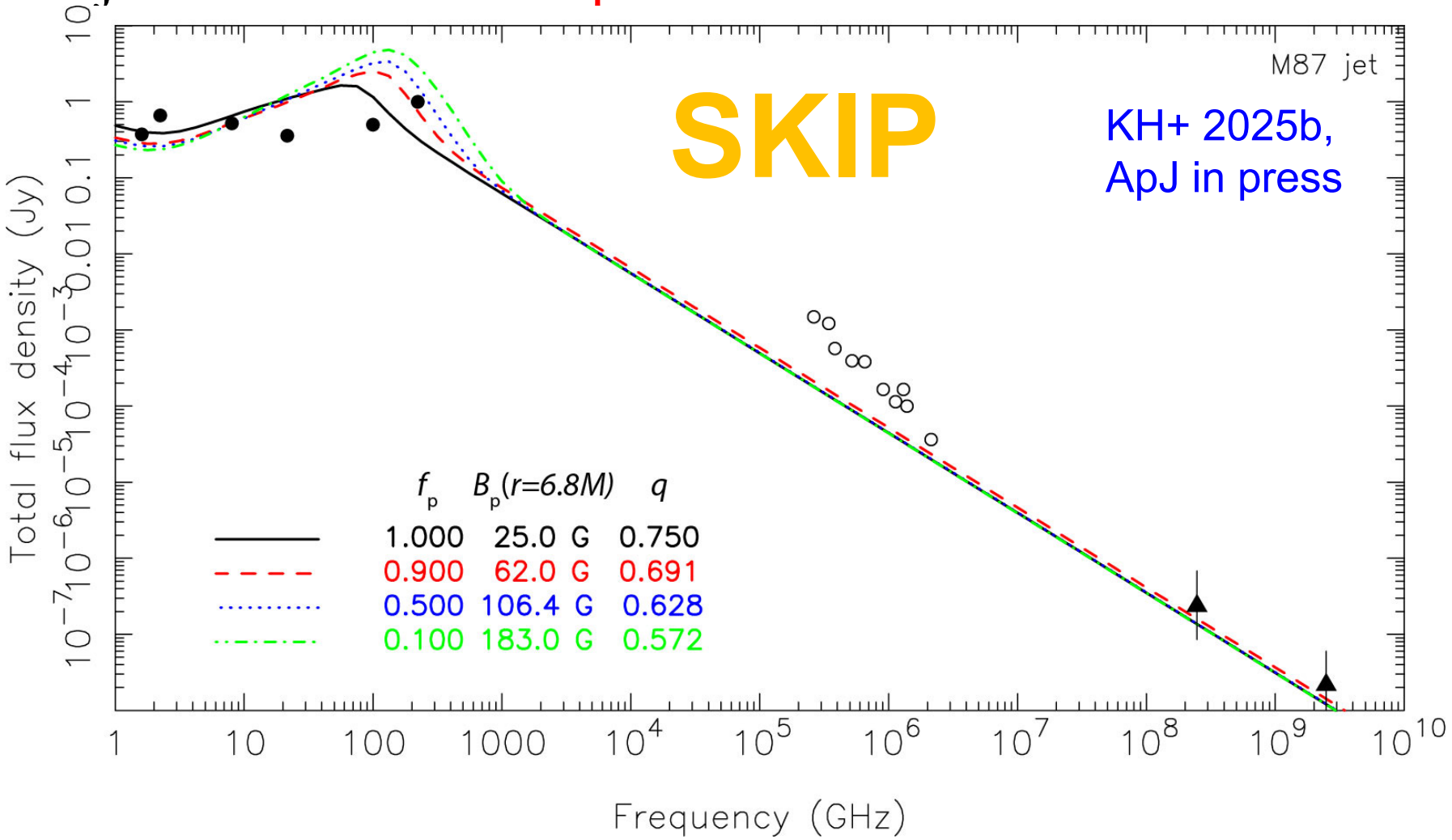

§ 4 *Implications for ALMA*

Lower frequency range (ALMA band 1) is important to find the deviation from a flat-top spectrum (< 10 GHz) to an inverted spectrum (> 10 GHz). → nonthermal fraction on *r*

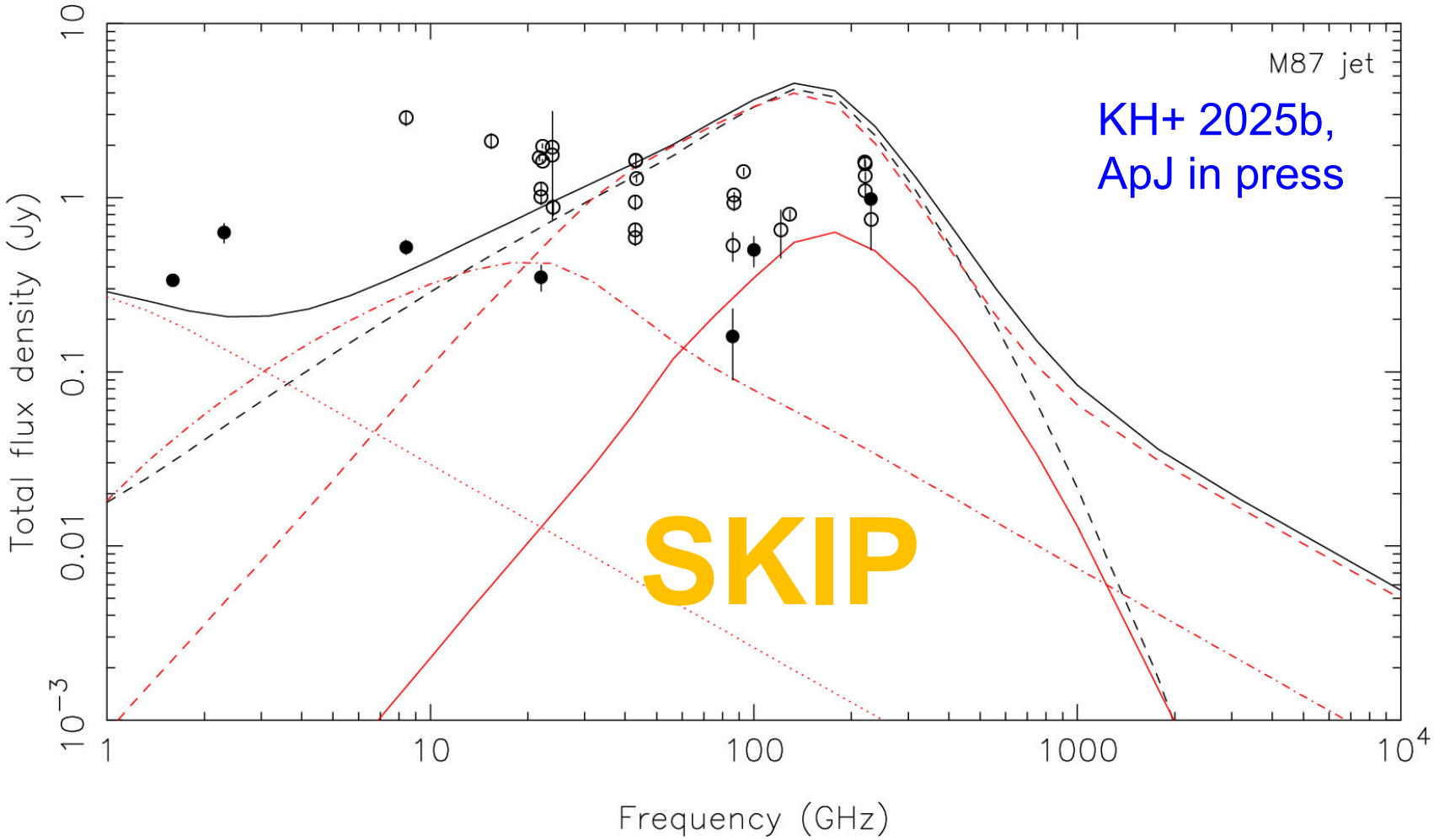

§ 4 *Implications for ALMA*

Middle frequency range (bands 2–8) constrains the curvature of the thermal component. → kT_e at jet base

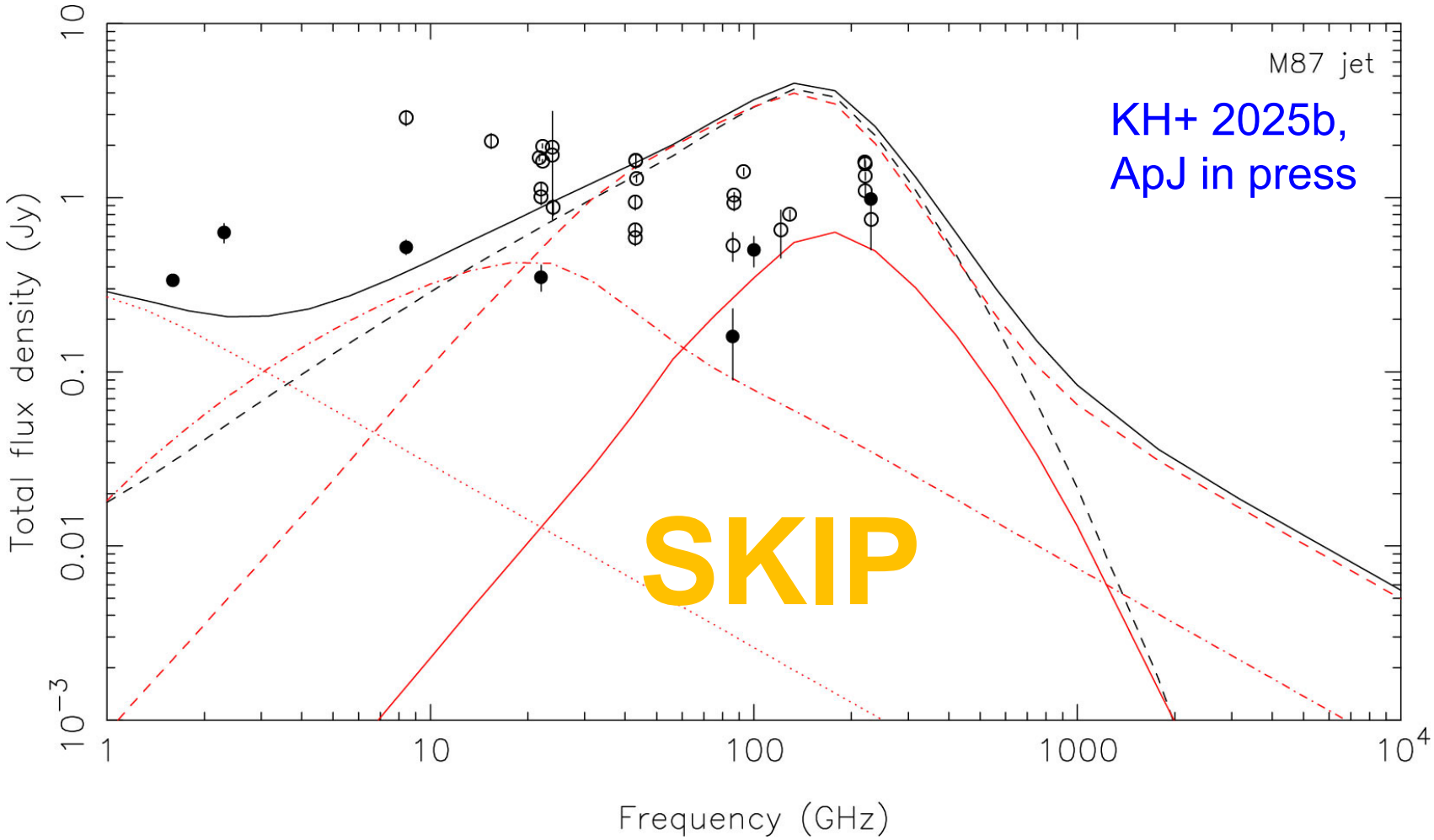

§ 4 *Implications for ALMA*

The higher frequency range (band 9–10) is important to constrain the inflection point, which is formed by thermal and nonthermal components. → B, q at jet base

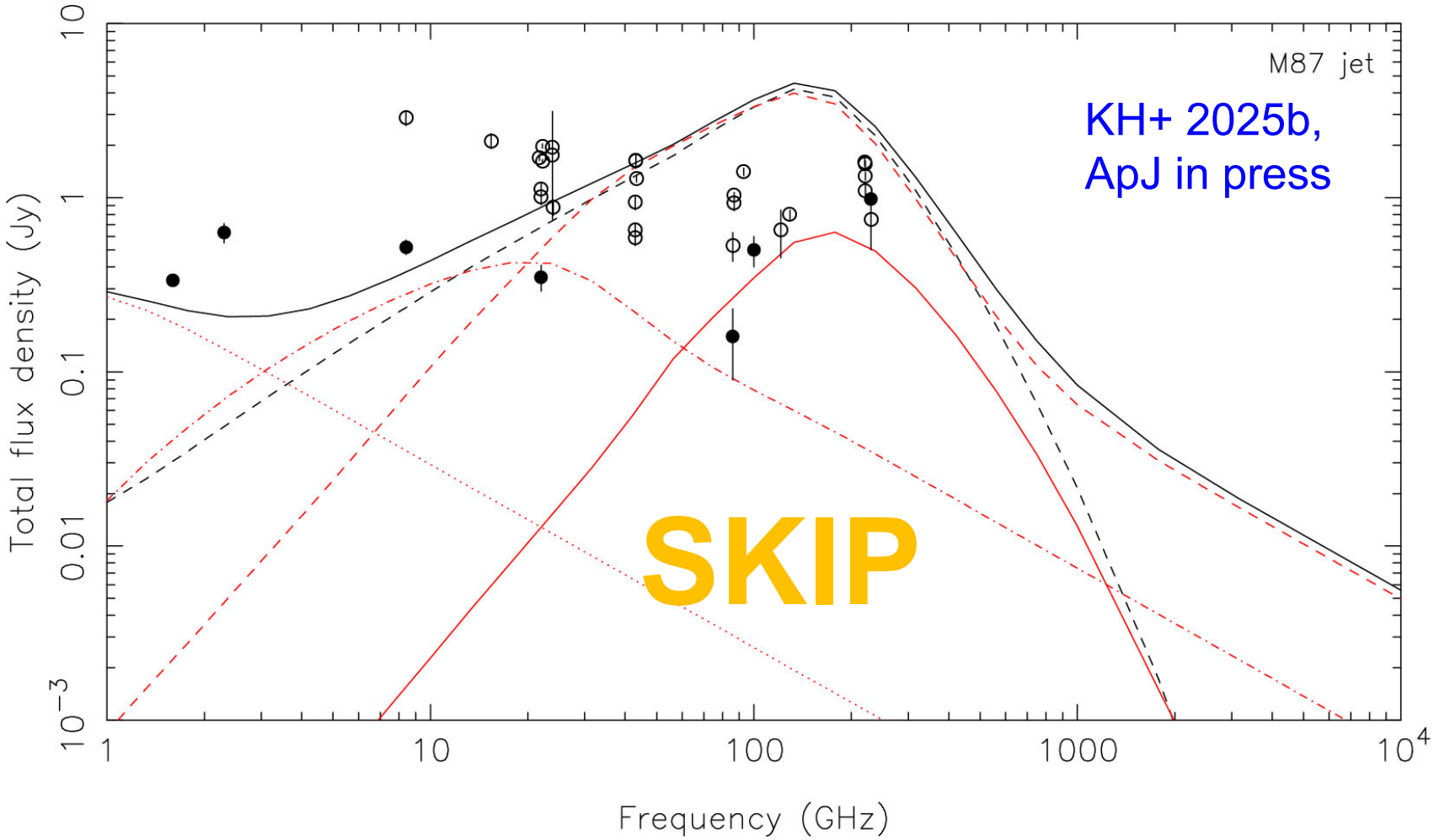

§ 4 *Implications for ALMA*

What is more, VLBI observations of the jet-launching region can independently constrain q (collimation index) using the opening angle, together with the viewing angle.

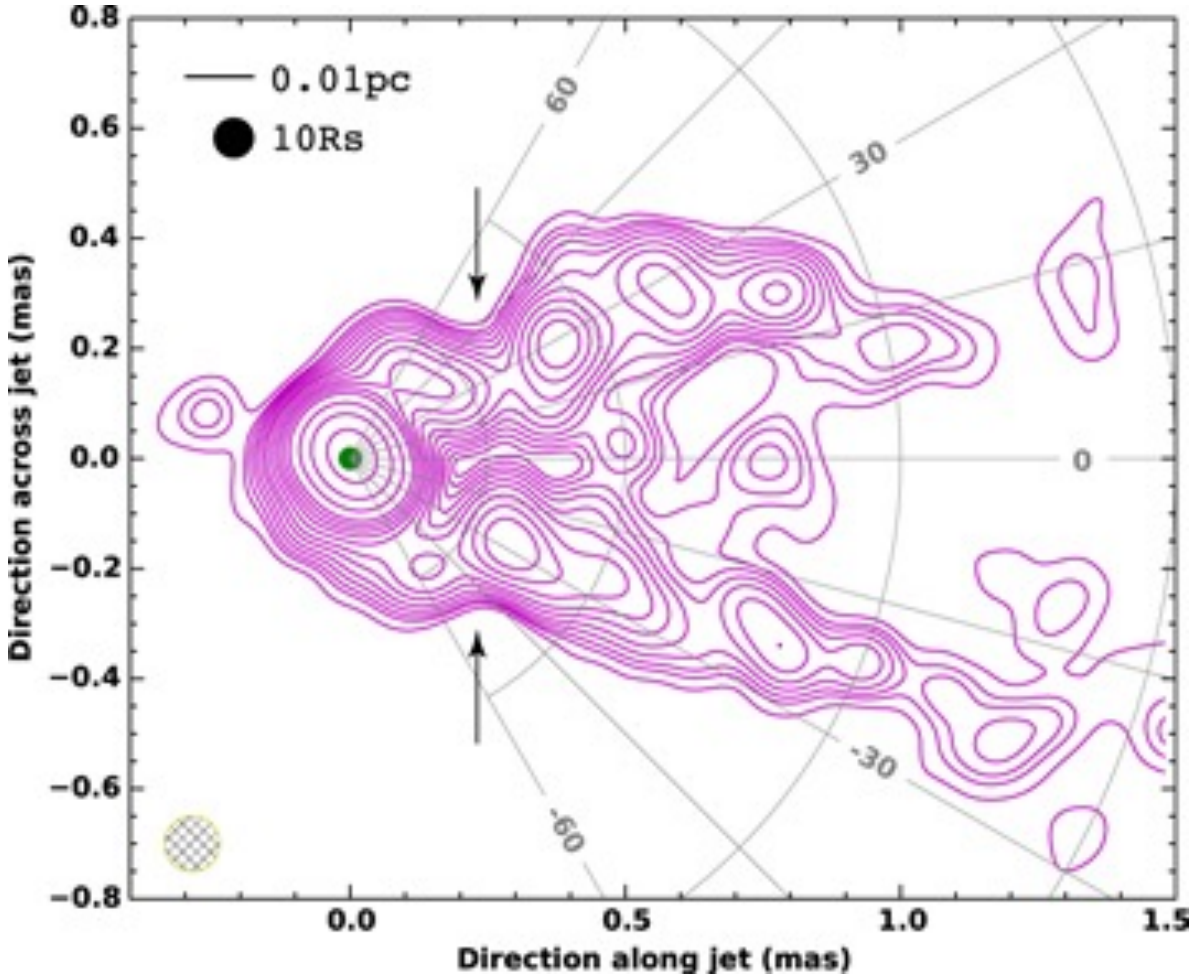

Hada +, 2016, ApJ **817** 131

Summary and Discussion

Comparing these observables with theoretical predictions obtained with our **R-JET** code, we can quantitatively constrain the matter content, collimation index (q), ***B*** field strength, plasma density, temperature, and nonthermal fraction at the base of AGN jets.

"*R-JET: A postprocessing code for radiative transport in relativistic jets*" KH + 2025a, ApJ 984, 16.

"*Constraining AGN jets with spectrum and core shift: the case of M87*" KH + 2025b, ApJ in press.